LETTER

doi:10.1038/nature10461

Laser cooling of a nanomechanical oscillator into its quantum ground state

Jasper Chan[1], T. P. Mayer Alegre[1]†, Amir H. Safavi-Naeini[1], Jeff T. Hill[1], Alex Krause[1], Simon Gröblacher[1,2], Markus Aspelmeyer[2] & Oskar Painter[1]

The simple mechanical oscillator, canonically consisting of a coupled mass–spring system, is used in a wide variety of sensitive measurements, including the detection of weak forces[1] and small masses[2]. On the one hand, a classical oscillator has a well-defined amplitude of motion; a quantum oscillator, on the other hand, has a lowest-energy state, or ground state, with a finite-amplitude uncertainty corresponding to zero-point motion. On the macroscopic scale of our everyday experience, owing to interactions with its highly fluctuating thermal environment a mechanical oscillator is filled with many energy quanta and its quantum nature is all but hidden. Recently, in experiments performed at temperatures of a few hundredths of a kelvin, engineered nanomechanical resonators coupled to electrical circuits have been measured to be oscillating in their quantum ground state[3,4]. These experiments, in addition to providing a glimpse into the underlying quantum behaviour of mesoscopic systems consisting of billions of atoms, represent the initial steps towards the use of mechanical devices as tools for quantum metrology[5,6] or as a means of coupling hybrid quantum systems[7–9]. Here we report the development of a coupled, nanoscale optical and mechanical resonator[10] formed in a silicon microchip, in which radiation pressure from a laser is used to cool the mechanical motion down to its quantum ground state (reaching an average phonon occupancy number of 0.85 ± 0.08). This cooling is realized at an environmental temperature of 20 K, roughly one thousand times larger than in previous experiments and paves the way for optical control of mesoscale mechanical oscillators in the quantum regime.

It has been known for some time[11] that atoms and ions nearly resonant with an applied laser beam (or series of beams) may be mechanically manipulated—even trapped and cooled down to the quantum ground state of their centre-of-mass motion[12]. Equally well known[1] is the fact that radiation pressure can be exerted on ordinary (that is, non-resonant) dielectric objects to damp and cool their mechanical motion. In 'cavity-assisted' schemes, the radiation pressure force is enhanced by coupling the motion of a mechanical object to the electromagnetic field in a resonant cavity. Pumping of the cavity by a single-frequency electromagnetic source produces a coupling between the mechanical motion and the intensity of the electromagnetic field built up in the resonator. Because the radiation pressure force exerted on the mechanical object is proportional to the field intensity in the resonator, a form of dynamical back-action results[1,13]. For a lower-frequency ('red') detuning of the pump source from the cavity, this leads to damping and cooling of the mechanical motion.

Recent experiments involving micro- and nanomechanical resonators coupled to electromagnetic fields at optical and microwave frequencies have demonstrated significant dynamic back-action due to radiation pressure[13]. These structures have included Fabry–Pérot cavities with mechanically compliant miniature end mirrors[14–18] or internal nanomembranes[19], whispering-gallery glass resonators[20], nanowires capacitively coupled to co-planar microwave transmission line cavities[6,21] and lumped-circuit microwave resonators with deformable, nanoscale, vacuum-gap capacitors[22]. The first measurement of an engineered mesoscopic mechanical resonator predominantly in its quantum ground state, however, was performed not using back-action cooling but rather using conventional cryogenic cooling (bath temperature, $T_b \approx 25$ mK) of a high-frequency and, thus, low-thermal-occupancy oscillator[3]. Read-out and control of mechanical motion at the single-quantum level was performed by strongly coupling the gigahertz-frequency piezoelectric mechanical resonator to a resonant superconducting quantum circuit. Only recently have microwave systems, also operating at bath temperatures of $T_b \approx 25$ mK, used radiation pressure back-action to cool a high-Q-factor, megahertz-frequency mechanical oscillator to the ground state[4,21].

Optically coupled mechanical devices, although they allow for control of the mechanical system through well-established quantum optical techniques[23], have thus far not reached the quantum regime owing to a great number of technical difficulties[20]. A particular challenge has been maintaining efficient optical coupling and low-loss optics and mechanics in a cryogenic, subkelvin environment. The optomechanical system studied in this work allows large optical coupling to a high-Q, gigahertz-frequency mechanical oscillator, offering both efficient back-action cooling and significantly higher operating temperatures. As shown in Fig. 1a, the system consists of an integrated optical and mechanical nanoscale resonator formed in the surface layer of a silicon-on-insulator microchip. The periodic patterning of the nanobeam is designed to result in Bragg scattering of both optical and acoustic guided waves. A perturbation in the periodicity at the centre of the beam results in co-localized optical and mechanical resonances (Fig. 1b, c), which are coupled through radiation pressure[10]. The fundamental optical resonance of the structure occurs at a frequency of $\omega_o/2\pi = 195$ THz ($\lambda = 1{,}537$ nm), whereas, owing to the speed of sound being much less than the speed of light, the mechanical resonance occurs at $\omega_m/2\pi = 3.68$ GHz. To minimize mechanical damping in the structure, an external acoustic radiation shield is added in the periphery of the nanobeam (Fig. 1d, e). This shield consists of a two-dimensional 'cross' pattern, which has been shown both theoretically and experimentally to yield a substantial phononic bandgap in the gigahertz frequency band[24].

We use a fibre-taper nanoprobe, formed from standard single-mode optical fibre, to optically couple to the silicon nanoscale resonators. As shown in Fig. 2, a tunable laser (New Focus Velocity swept laser; 200-kHz linewidth) is used to cool optically and transduce the mechanical motion of the nanomechanical oscillator. Placing the optomechanical devices into a continuous-flow helium cryostat provides pre-cooling down to $T_b \approx 20$ K, reducing the bath occupancy of the 3.68-GHz mechanical mode to $n_b \approx 100$. At this temperature, the mechanical Q-factor increases up to a measured value of $Q_m \approx 10^5$, corresponding to an intrinsic mechanical damping rate of $\gamma_i/2\pi = 35$ kHz. The optical Q-factor is measured to be $Q_o = 4 \times 10^5$, corresponding to an optical linewidth of $\kappa/2\pi = 500$ MHz, slightly reduced from its room-temperature value.

[1]Thomas J. Watson, Sr, Laboratory of Applied Physics, California Institute of Technology, Pasadena, California 91125, USA. [2]Vienna Center for Quantum Science and Technology (VCQ), Faculty of Physics, University of Vienna, Boltzmanngasse 5, A-1090 Vienna, Austria. †Present address: Instituto de Física "Gleb Wataghin", Universidade Estadual de Campinas, UNICAMP, 13083-859, Campinas, SP, Brazil.

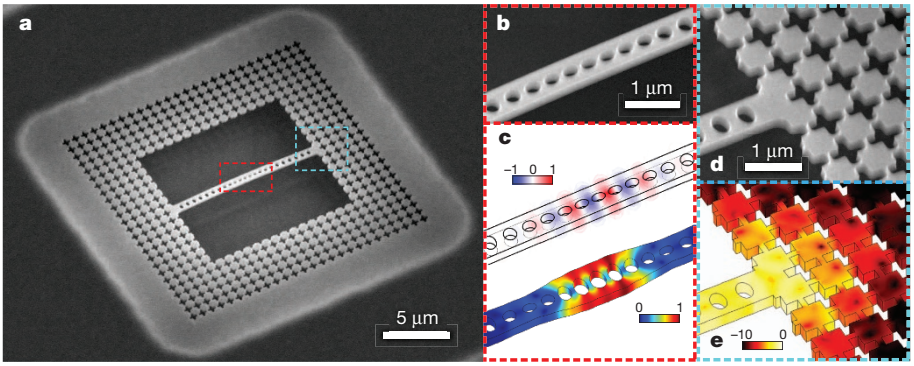

Figure 1 | Optomechanical resonator with phononic shield. **a**, Scanning electron microscope (SEM) image of the patterned silicon nanobeam and the external phononic bandgap shield. **b**, Enlarged SEM image of the central cavity region of the nanobeam. **c**, Top: normalized electric field (colour scale) of the localized optical resonance of the nanobeam cavity, simulated using the finite-element method (FEM). Bottom: FEM simulation of the normalized displacement field of the acoustic resonance (breathing mode), which is coupled by radiation pressure to the co-localized optical resonance. The displacement field is indicated by the exaggerated deformation of the structure, with the relative magnitude of the local displacement (strain) indicated by the colour. **d**, SEM image of the interface between the nanobeam and the phononic bandgap shield. **e**, FEM simulation of the normalized squared displacement field amplitude of the localized acoustic resonance at the nanobeam–shield interface, indicating the strong suppression of acoustic radiation provided by the phononic bandgap shield. The colour scale represents $\log[x^2/\max(x^2)]$, where x is the displacement field amplitude.

In the resolved-sideband limit, where $\omega_m/\kappa > 1$, driving the system with a laser (frequency, ω_l) tuned to the red side of the optical cavity (detuning, $\Delta \equiv \omega_o - \omega_l = \omega_m$), creates an optically induced damping, γ_{OM}, of the mechanical resonance[25]. In the weak-coupling regime ($\gamma_{OM} \ll \kappa$), the optical back-action damping is given by $\gamma_{OM} = 4g^2 n_c/\kappa$, where n_c is the average number of drive-laser photons stored in the cavity and g is the optomechanical coupling rate between the mechanical and optical modes. This coupling rate, g, is quantified as the shift in the optical resonance for an amplitude of motion equal to the zero-point fluctuation amplitude ($x_{zpf} = (\hbar/2m\omega_m)^{1/2}$, where m is the motional mass of the localized acoustic mode and $\hbar$ is Planck's constant divided by 2π). The optomechanical damping, which is a result of the preferential scattering of drive photons into the upper-frequency sideband, also cools the mechanical mode. For a quantum-limited drive laser, the phonon occupancy of the mechanical oscillator can be reduced from $n_b = k_B T_b/\hbar\omega_m \gg 1$ to $\bar{n} = n_b/(1+C) + n_{min}$, where k_B is Boltzmann's constant and $C \equiv \gamma_{OM}/\gamma_i$ is the cooperativity. The residual scattering of drive photons into the lower-frequency sideband limits the cooled phonon occupancy to $n_{min} = (\kappa/4\omega_m)^2$, which is determined by the level of sideband resolution[25].

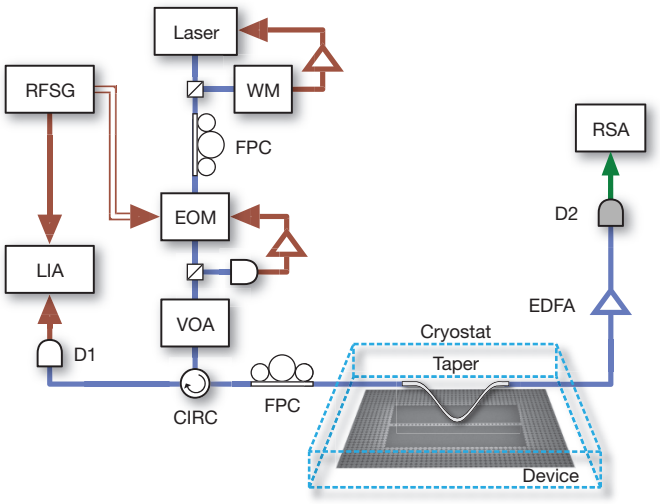

Figure 2 | Experimental set-up. A single, tunable, 1,550-nm diode laser is used as the cooling and mechanical transduction beam sent into the nanobeam optomechanical resonator cavity held in a continuous-flow helium cryostat. A wavemetre (WM) is used to track and lock the laser frequency, and a variable optical attenuator (VOA) is used to set the laser power. The transmitted signal is amplified by an erbium-doped fibre amplifier (EDFA) and detected on a high-speed photodetector (D2) connected to a real-time spectrum analyser (RSA), where the mechanical noise power spectrum is measured. A slowly modulated probe signal used for optical spectroscopy and calibration is generated from the cooling laser beam using an amplitude electro-optic modulator (EOM) driven by a microwave source (RFSG). The reflected component of this signal is separated from the input by an optical circulator (CIRC), sent to a photodetector (D1) and then demodulated using a lock-in amplifier (LIA). Paddle-wheel fibre polarization controllers (FPCs) are used to set the laser polarization at the input to the EOM and the input to the optomechanical cavity. For more detail, see Supplementary Information.

The drive laser, in addition to providing mechanical damping and cooling, can be used to measure the mechanical and optical properties of the system through a series of calibrated measurements. In a first set of measurements, we use the noise power spectral density (PSD) of the drive laser transmitted through the optomechanical cavity to perform spectroscopy of the mechanical mode. As shown in Supplementary Information, the noise PSD of the photocurrent generated by the transmitted field of the drive laser with red-sideband detuning ($\Delta = \omega_m$) yields a Lorentzian component of the single-sided PSD proportional to $S_b(\omega) = \bar{n}\gamma/\left((\omega-\omega_m)^2 + (\gamma/2)^2\right)$, where $\gamma = \gamma_i + \gamma_{OM} = \gamma_i(1+C)$ is the total mechanical damping rate. For a blue laser detuning of $\Delta = -\omega_m$, the optically induced damping is negative ($\gamma_{OM} = -4g^2 n_c/\kappa$) and the photocurrent noise PSD is proportional to $S_{b\dagger}(\omega) = (\bar{n}+1)\gamma/\left((\omega-\omega_m)^2 + (\gamma/2)^2\right)$. Typical measured noise power spectra under low-power laser drive ($n_c = 1.4$, $C = 0.27$), for both red detuning and blue detuning, are shown in Fig. 3a. Even at these small drive powers, the effects of back-action on the measured spectra are evident, with the red-detuned drive broadening the mechanical line and the blue-detuned drive narrowing the line. The noise floor in Fig. 3a (shaded in grey) corresponds to the noise generated by the EDFA used to pre-amplify the transmitted drive-laser signal before photodetection, and is several orders of magnitude greater than the electronic noise of the photoreceiver and the real-time spectrum analyser.

Calibration of the EDFA gain, along with the photoreceiver and real-time spectrum analyser photodetection gain, makes it possible to convert the measured area under the photocurrent noise PSD into a mechanical mode phonon occupancy. As described in detail in Supplementary Information, we perform these calibrations, along with measurements of low-drive-power ($C \ll 1$), radio-frequency spectra of both detunings ($\Delta = \pm\omega_m$), to provide accurate, local thermometry of the optomechanical cavity. An example of this form of calibrated mode thermometry is shown in Fig. 3b, where we plot the optically measured

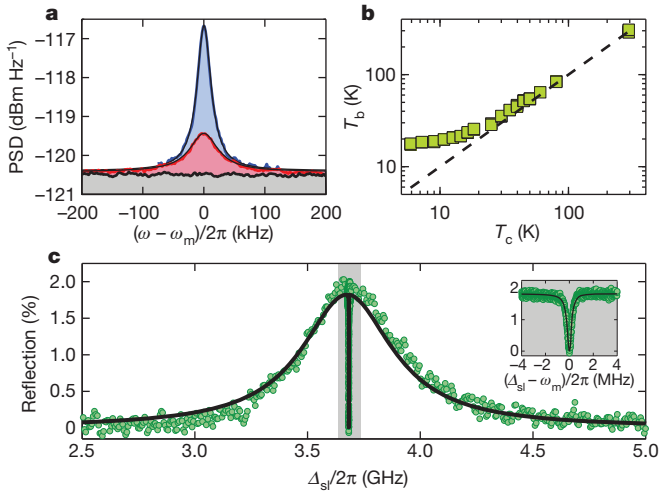

Figure 3 | Mechanical and optical response. **a**, Typical measured mechanical noise spectra around the resonance frequency of the breathing mode for low drive-laser power ($n_c = 1.4$). The blue and red curves correspond to the spectra measured with the drive laser blue- and, respectively, red-detuned by a mechanical frequency from the optical cavity resonance. The black trace corresponds to the measured noise floor (dominated by EDFA noise) with the drive laser detuned far from the cavity resonance. **b**, Plot of the measured (squares) mechanical mode bath temperature (T_b) as a function of cryostat sample mount temperature (T_c). The dashed line indicates the curve corresponding to perfect following of the cryostat temperature by the mode temperature ($T_b = T_c$). **c**, Typical reflection spectrum (normalized power reflection) of the cavity while driven by the cooling laser ($\Delta = \omega_m$, $n_c = 56$, $C = 11$), as measured by a weaker probe beam at two-photon detuning Δ_{sl}. The signature reflection dip on resonance with the bare cavity mode, highlighted in the inset, is indicative of EIT caused by coupling of the optical and mechanical degrees of freedom by the cooling laser beam.

mechanical mode bath temperature, T_b, as a function of the cryostat sample mount temperature, T_c (independently measured using a silicon diode thermometer attached to the copper sample mount). Figure 3b shows that the optical mode thermometry predicts a mode temperature in good correspondence with the absolute temperature of the sample mount for $T_c > 50$ K; below this value, the mode temperature deviates from T_c and saturates to a value of $T_b = 17.6 \pm 0.8$ K owing to thermal radiative heating of the device through the imaging aperture in the radiation shield of our cryostat.

In a second set of measurements, we determine the mechanical damping, γ, and the cavity–laser detuning, Δ, by optical spectroscopy of the driven cavity. By sweeping a second probe beam, of frequency ω_s, over the cavity, with the cooling beam tuned to $\Delta = \omega_m$, spectra showing electromagnetically induced transparency[26] (EIT) are measured (Fig. 3c). Owing to the high single-photon cooperativity of the system, an intracavity population of only $n_c \approx 5$ switches the system from reflecting to transmitting for the probe beam. The corresponding dip at the centre of the optical cavity resonance occurs at a two-photon detuning of $\Delta_{sl} \equiv \omega_s - \omega_l = \omega_m$ and has a bandwidth equal to the mechanical damping rate, $\gamma_i(1 + C)$. In Fig. 4a, we plot the measured mechanical linewidth as a function of intracavity photon number, showing good correspondence between both mechanical and optical spectroscopy techniques, and indicating that the system remains in the weak-coupling regime for all measured cooling powers. From a fit to the measured mechanical damping rate as a function of n_c (Fig. 4a, dashed red line), the zero-point optomechanical coupling rate is determined to be $g/2\pi = 910$ kHz.

In Fig. 4b, we plot the calibrated Lorentzian noise PSD area, in units of phonon occupancy, as a function of red-detuned ($\Delta = \omega_m$) drive-laser power. Owing to the low effective temperature of the laser drive, the mechanical mode is not only damped but is also cooled substantially. The minimum measured average mode occupancy for the highest drive power (corresponding to $n_c \approx 2{,}000$) is $\bar{n} = 0.85 \pm 0.08$, putting the mechanical oscillator in a thermal state with ground-state occupancy probability greater than 50%. The dashed blue line in Fig. 4b represents the ideal back-action-cooled phonon occupancy estimated using both the measured mechanical damping rate in Fig. 4a and the low-drive-power intrinsic mechanical damping rate. Deviation of the measured phonon occupancy from the ideal cooling model is seen to

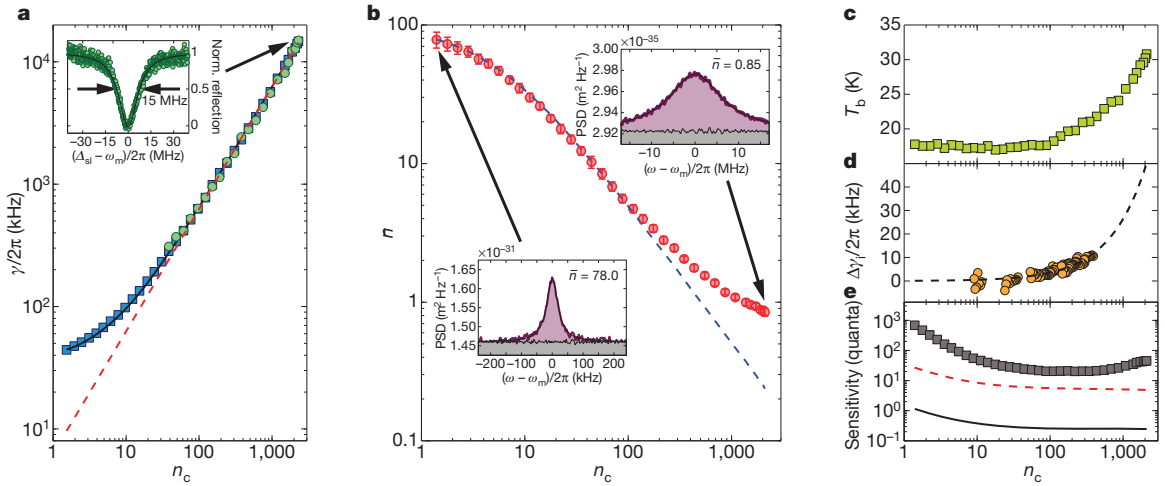

Figure 4 | Optical cooling results. **a**, Measured mechanical mode linewidth (squares), EIT transparency bandwidth (circles) and predicted optomechanical damping rate estimated using the zero-point optomechanical coupling rate, $g/2\pi = 910$ kHz (red dashed line). Inset, measured EIT transparency window at the highest cooling-beam drive power. **b**, Measured (circles) average phonon number, $\bar{n}$, in the breathing mechanical mode at $\omega_m/2\pi = 3.68$ GHz, versus cooling drive-laser power (in units of intracavity photons, n_c), as deduced from the calibrated area under the Lorentzian line shape of the mechanical noise power spectrum. The inset spectra show the measured noise PSD (using $x_{zpf} = 2.7$ fm, corresponding to the numerically computed motional mass for the breathing mode with $m = 311$ fg). The dashed blue line indicates the estimated mode phonon number calculated from the measured optical damping alone. Error bars indicate estimated uncertainties as outlined in Supplementary Information. **c**, Estimated bath temperature, T_b, versus cooling laser intracavity photon number, n_c. **d**, Measured change in the intrinsic mechanical damping rate versus n_c (circles). A polynomial fit to the mechanical damping dependence on n_c is shown as a dashed line. For more details, see Supplementary Information. **e**, The measured (squares) background noise PSD versus drive-laser power (n_c), in units of effective phonon quanta. The red dashed curve corresponds to the theoretical imprecision assuming shot-noise-limited detection but all other cavity properties and optical loss as in the experiment. The solid black curve is for an ideal, quantum-limited continuous position measurement of mechanical motion.

occur at the highest drive powers and results from both an increase in the bath temperature due to optical absorption (Fig. 4c) and an increase in the intrinsic mechanical damping rate (Fig. 4d) induced by the generation of free carriers through optical absorption (Supplementary Information). To evaluate the efficiency of the optical transduction of the mechanical motion, we also plot (Fig. 4e) the measured background noise PSD, or imprecision level. The minimum measured imprecision, occurring for $n_c \approx 500$ corresponds to $n_{imp} \approx 20$ in units of phonon quanta when referred to the peak Lorentzian level of the transduced mechanical motion (Supplementary Information). Comparing the measured imprecision with the respective theoretical imprecision levels for shot-noise-limited detection (Fig. 4e, dashed red curve) and ideal quantum-limited motion transduction (Fig. 4e, black curve) indicates that $n_{imp}^{EDFA} \approx 15$ stems from the excess noise imparted by the EDFA optical amplifier. The remaining $n_{imp}^{loss} \approx 5$ is due to optical loss of signal inside the cavity (11.7 dB) and in the optical fibre output waveguide (2 dB).

Looking forward, the optical back-action cooling and thermometry, as performed in this work, represents only a first step towards optical measurement and control of the quantum state of a nanomechanical object. The mechanical system, although cooled to a mode occupancy of less than one, is still prepared in a classical thermal state, with its quantum zero-point fluctuations hidden by our measurement scheme. However, experiments to prepare and measure non-classical quantum states of the mechanical system are now within reach. A basic requirement for optomechanical experiments in the quantum regime is the ability to exchange photons with the mechanical resonator on a timescale shorter than that for a single thermal phonon to enter the mechanical system from the environment. The latter, called the thermal decoherence time, is given by $\tau_{th} \equiv \hbar Q_m / k_B T_b$, and the timescale on which the mechanical resonator exchanges photons with an optical input is $\tau_{OM} \equiv 1/\gamma_{OM}$. The requirement that $\tau_{OM} < \tau_{th}$ is equivalent to the requirement for optical back-action cooling of the mechanical oscillator to $\bar{n} < 1$, and is thus realized for the optomechanical crystal devices reported here. This allows for optomechanical entanglement between light and mechanics[27] or quantum state transfer between single optical photons and mechanical phonons[9,28], enabling mechanical systems to function as both quantum transducers[8] and quantum memory elements[29]. In addition, the chip-scale nature of the optomechanical crystal architecture naturally lends itself to the creation of coupled photon–phonon circuits, facilitating not only the coupling of multiple mechanical and optical objects, but also allowing for the integration of optomechanics with other quantum systems such as superconducting quantum circuits[9]. Finally, if a regime of strong coupling at the single-quantum level[30] ($g/\kappa > 1$) could be reached, many new opportunities would be available, not least the study of nonlinear phononics at the single-phonon level and the generation of highly non-classical quantum states in mechanical or optical systems.

Received 17 June; accepted 16 August 2011.

1. Braginsky, V. & Manukin, A. *Measurement of Weak Forces in Physics Experiments* (Univ. Chicago Press, 1977).
2. Jensen, K., Kim, K. & Zettl, A. An atomic-resolution nanomechanical mass sensor. *Nature Nanotechnol.* **3,** 533–537 (2008).
3. O'Connell, A. D. *et al.* Quantum ground state and single-phonon control of a mechanical resonator. *Nature* **464,** 697–703 (2010).
4. Teufel, J. D. *et al.* Sideband cooling of micromechanical motion to the quantum ground state. *Nature* **475,** 359–363 (2011).
5. Caves, C., Thorne, K., Drever, R., Sandberg, V. D. & Zimmermann, M. On the measurement of a weak classical force coupled to a quantum-mechanical oscillator. *Rev. Mod. Phys.* **52,** 341–392 (1980).
6. Regal, C. A., Teufel, J. D. & Lehnert, K. W. Measuring nanomechanical motion with a microwave cavity interferometer. *Nature Phys.* **4,** 555–560 (2008).
7. Wallquist, M., Hammerer, K., Rabl, P., Lukin, M. & Zoller, P. Hybrid quantum devices and quantum engineering. *Phys. Scr.* **2009,** 014001 (2009).
8. Stannigel, K., Rabl, P., Sørensen, A. S., Zoller, P. & Lukin, M. D. Optomechanical transducers for long-distance quantum communication. *Phys. Rev. Lett.* **105,** 220501 (2010).
9. Safavi-Naeini, A. H. & Painter, O. Proposal for an optomechanical traveling wave phonon-photon translator. *N. J. Phys.* **13,** 013017 (2011).
10. Eichenfield, M., Chan, J., Camacho, R. M., Vahala, K. J. & Painter, O. Optomechanical crystals. *Nature* **462,** 78–82 (2009).
11. Cohen-Tannoudji, C. N. & Phillips, W. D. New mechanisms for laser cooling. *Phys. Today* **43,** 33–40 (1990).
12. Diedrich, F., Bergquist, J. C., Itano, W. M. & Wineland, D. J. Laser cooling to the zero-point energy of motion. *Phys. Rev. Lett.* **62,** 403–406 (1989).
13. Kippenberg, T. J. & Vahala, K. J. Cavity optomechanics: back-action at the mesoscale. *Science* **321,** 1172–1176 (2008).
14. Cohadon, P.-F., Heidmann, A. & Pinard, M. Cooling of a mirror by radiation pressure. *Phys. Rev. Lett.* **83,** 3174–3177 (1999).
15. Metzger, C. H. & Karrai, K. Cavity cooling of a microlever. *Nature* **432,** 1002–1005 (2004).
16. Gigan, S. *et al.* Self-cooling of a micromirror by radiation pressure. *Nature* **444,** 67–70 (2006).
17. Arcizet, O., Cohadon, P.-F., Briant, T., Pinard, M. & Heidmann, A. Radiation-pressure cooling and optomechanical instability of a micromirror. *Nature* **444,** 71–74 (2006).
18. Gröblacher, S. *et al.* Demonstration of an ultracold micro-optomechanical oscillator in a cryogenic cavity. *Nature Phys.* **5,** 485–488 (2009).
19. Thompson, J. D. *et al.* Strong dispersive coupling of a high-finesse cavity to a micromechanical membrane. *Nature* **452,** 72–75 (2008).
20. Rivière, R. *et al.* Optomechanical sideband cooling of a micromechanical oscillator close to the quantum ground state. *Phys. Rev. A* **83,** 063835 (2011).
21. Rocheleau, T. *et al.* Preparation and detection of a mechanical resonator near the ground state of motion. *Nature* **463,** 72–75 (2010).
22. Teufel, J. D. *et al.* Circuit cavity electromechanics in the strong-coupling regime. *Nature* **471,** 204–208 (2011).
23. Wiseman, H. M. & Milburn, G. J. *Quantum Measurement and Control* (Cambridge Univ. Press, 2010).
24. Alegre, T. P. M., Safavi-Naeini, A., Winger, M. & Painter, O. Quasi-two-dimensional optomechanical crystals with a complete phononic bandgap. *Opt. Express* **19,** 5658–5669 (2011).
25. Marquardt, F., Chen, J. P., Clerk, A. A. & Girvin, S. M. Quantum theory of cavity-assisted sideband cooling of mechanical motion. *Phys. Rev. Lett.* **99,** 093902 (2007).
26. Safavi-Naeini, A. H. *et al.* Electromagnetically induced transparency and slow light with optomechanics. *Nature* **472,** 69–73 (2011).
27. Vitali, D. *et al.* Optomechanical entanglement between a movable mirror and a cavity field. *Phys. Rev. Lett.* **98,** 030405 (2007).
28. Akram, U., Kiesel, N., Aspelmeyer, M. & Milburn, G. J. Single-photon optomechanics in the strong coupling regime. *N. J. Phys.* **12,** 083030 (2010).
29. Chang, D., Safavi-Naeini, A. H., Hafezi, M. & Painter, O. Slowing and stopping light using an optomechanical crystal array. *N. J. Phys.* **13,** 023003 (2011).
30. Rabl, P. Photon blockade effect in optomechanical systems. *Phys. Rev. Lett.* **107,** 063601 (2011).

Supplementary Information is linked to the online version of the paper at www.nature.com/nature.

Acknowledgements This work was supported by the DARPA/MTO ORCHID program through a grant from the AFOSR, the European Commission (MINOS, QUESSENCE), the European Research Council (ERC QOM), the Austrian Science Fund (CoQuS, FOQUS, START) and the Kavli Nanoscience Institute at the California Institute of Technology. The authors thank B. Baker for help with the cryostat set-up, J.C. thanks R. Li, and J.C. and A.H.S.-N. acknowledge support from NSERC.

Author Contributions J.C., T.P.M.A. and A.H.S.-N. designed the device, and J.C. fabricated it with support from J.T.H. J.C., T.P.M.A., A.H.S.-N., J.T.H., A.K. and S.G. performed the measurements and analysed the measured data. O.P. and M.A. supervised the measurements and the data analysis. All authors contributed to the writing of the manuscript.

Author Information Reprints and permissions information is available at www.nature.com/reprints. The authors declare no competing financial interests. Readers are welcome to comment on the online version of this article at www.nature.com/nature. Correspondence and requests for materials should be addressed to O.P. (opainter@caltech.edu).